nature biotechnology

Article

https://doi.org/10.1038/s41587-022-01649-9

Precise transcript targeting by CRISPR-Csm complexes

Received: 1 June 2022

Accepted: 15 December 2022

Published online: 23 January 2023

Check for updates

David Colognori[1,2], Marena Trinidad[1,2] & Jennifer A. Doudna[1,3,4,5,6,7]

Robust and precise transcript targeting in mammalian cells remains a difficult challenge using existing approaches due to inefficiency, imprecision and subcellular compartmentalization. Here we show that the clustered regularly interspaced short palindromic repeats (CRISPR)-Csm complex, a multiprotein effector from type III CRISPR immune systems in prokaryotes, provides surgical RNA ablation of both nuclear and cytoplasmic transcripts. As part of the most widely occurring CRISPR adaptive immune pathway, CRISPR-Csm uses a programmable RNA-guided mechanism to find and degrade target RNA molecules without inducing indiscriminate *trans*-cleavage of cellular RNAs, giving it an important advantage over the CRISPR-Cas13 family of enzymes. Using single-vector delivery of the *Streptococcus thermophilus* Csm complex, we observe high-efficiency RNA knockdown (90–99%) and minimal off-target effects in human cells, outperforming existing technologies including short hairpin RNA- and Cas13-mediated knockdown. We also find that catalytically inactivated Csm achieves specific and durable RNA binding, a property we harness for live-cell RNA imaging. These results establish the feasibility and efficacy of multiprotein CRISPR-Cas effector complexes as RNA-targeting tools in eukaryotes.

The ability to alter RNA and protein levels in cells and organisms without making permanent changes to DNA has proven invaluable for both basic research and therapeutics. For the past two decades, targeted RNA knockdown (KD) in eukaryotes has been accomplished using RNA interference (RNAi), an approach whereby small interfering RNAs (siRNAs) direct endogenous Argonaute nucleases to cleave complementary target RNAs[1,2]. However, RNAi can cause unintended cleavage of targets carrying partial sequence complementarity, especially when this complementarity occurs within the nucleating 'seed' region of the siRNA[3–5]. Furthermore, siRNAs are inefficient at targeting nuclear RNAs because the RNAi machinery localizes primarily to the cytoplasm[6,7]. Finally, RNAi is incompatible with certain eukaryotic model systems, including budding yeast that lacks RNAi machinery[8,9] and zebrafish embryos that suffer from nonspecific developmental defects[10,11]. Thus, there has been ongoing interest in developing new RNA KD tools with higher specificity and broader targeting capability.

Clustered regularly interspaced short palindromic repeats (CRISPR)-CRISPR-associated proteins (Cas), which comprise adaptive defense systems against infectious agents in prokaryotes[12,13], operate as programmable DNA or RNA nucleases[14–16]. Similar to RNAi, Cas nucleases use small RNAs, or CRISPR RNAs (crRNAs), to recognize nucleic acid targets via base-pairing complementarity. One such nuclease, Cas13, has gained attention as a new RNA-cleavage tool for use in eukaryotes[17–19]. However, unlike Argonaute proteins that cut only complementary RNAs in *cis*[20], Cas13 also degrades nearby noncomplementary RNAs in *trans*[18,21] (Fig. 1a). This is because the nuclease domains of Cas13 are located away from the crRNA:target binding pocket on an exposed surface of the protein[22–25]. Cas13's *trans*-cleavage activity is readily detectable in vitro, where it has been exploited for viral RNA

[1]Department of Molecular and Cell Biology, University of California, Berkeley, CA, USA. [2]Innovative Genomics Institute, University of California, Berkeley, CA, USA. [3]Howard Hughes Medical Institute, University of California, Berkeley, CA, USA. [4]Department of Chemistry, University of California, Berkeley, CA, USA. [5]California Institute for Quantitative Biosciences (QB3), University of California, Berkeley, CA, USA. [6]Molecular Biophysics and Integrated Bioimaging Division, Lawrence Berkeley National Laboratory, Berkeley, CA, USA. [7]Gladstone Institutes, San Francisco, CA, USA. e-mail: doudna@berkeley.edu

detection tools[21,26–29]. In bacteria, *trans*-cleavage leads to stalled cell growth or cell death (abortive infection)[30], which is now believed to be Cas13's primary mode of defensive action against viral infection. Only recently, however, has evidence mounted that Cas13 exhibits *trans*-cleavage activity in eukaryotic cells, causing cytotoxicity and/or cell death[31–35]. The convolution of *cis*- and *trans*-cutting effects has made it difficult to interpret results obtained using Cas13, and call into question its utility as a tool for specific RNA KD.

Despite their higher prevalence in nature[36], multisubunit Cas effectors have been harnessed only rarely as tools in eukaryotes (with few exceptions[37–39]) compared to single-subunit effectors, due to their component complexity. Nonetheless, the well-studied biochemical and structural properties of type III RNA-targeting CRISPR-Csm complexes make them of particular interest for potential transcript targeting tools. The multiprotein Csm complex comprises five subunits (Csm1-5) in varying stoichiometries and relies on an additional protein, Cas6, for processing the precursor crRNA[40–47] (Fig. 1b). The crRNA lies at the core of the complex, with Csm1 and Csm4 binding the 5′ end, Csm5 binding the 3′ end and multiple copies of Csm2 and Csm3 wrapping around the center. The complex contains a groove along its length into which target RNAs can enter and hybridize to the variable spacer region of the crRNA. Csm1 and Csm4 specifically recognize the 5′ region of the crRNA derived from the CRISPR repeat. Each Csm3 subunit has ribonuclease (RNase) activity, leading to multiple cleavage sites within the target RNA spaced six nucleotides (nt) apart (Fig. 1c). Csm1 functions as a nonspecific single-stranded DNase (ssDNase)[48,49] and a cyclic oligoadenylate (cA) synthase[50,51] (Fig. 1b). The ssDNase activity is thought to defend against actively transcribed (R-looped) or ssDNA foreign genomes[48,49], while the latter acts as a second messenger that activates downstream effectors in *trans*, such as the RNase Csm6 (refs. [50,51]). Notably, all three catalytic activities are performed by independent domains of the Csm complex and can be individually ablated.

Csm is an attractive RNA KD tool over current methods. A self-contained system found only in prokaryotes, it can be orthogonally introduced into eukaryotes without intersecting host RNA regulatory pathways. Furthermore, unlike RNAi, it can be localized to the nucleus and used to target nuclear noncoding RNAs and pre-mRNAs. Compared to Cas13, Csm cleaves only in *cis* within the crRNA:target complementary region and thus does not suffer from *trans*-cleavage activity[40]. Additionally, unlike Cas13, Csm-mediated RNA cleavage does not preferentially occur at a particular nt base (for example, U)[18,27] nor is directly influenced by sequence flanking the target (for example, tag:antitag complementarity)[43,52]. In this work, we demonstrate the utility of the Csm system as a highly efficient, specific and versatile RNA KD tool in eukaryotes.

Results

An all-in-one type III CRISPR-Cas system in human cells

We chose the type III-A Csm complex from *Streptococcus thermophilus* for several reasons as follows: (1) it has been extensively characterized biochemically, structurally and in bacteria[40–47], (2) it functions optimally at 37 °C, (3) it has been demonstrated to work in zebrafish embryos and human cell culture upon ribonucleoprotein (RNP) delivery[53,54] and (4) it has fewer components than the analogous type III-B Cmr complex[55]. We began by verifying proper expression of each individual protein component (Csm1-5 and Cas6) in immortalized human embryonic kidney (HEK293T) cells. Proteins were human codon optimized, N-terminally FLAG-tagged for detection and expressed from a cytomegalovirus promoter. While RNAi operates in the cytoplasm where mRNAs mainly reside, we chose to localize Cas6 and each Csm component to the nucleus through the addition of an N-terminal SV40 nuclear localization signal so as to target nuclear RNAs and pre-mRNAs before export. Following transient transfection, Western blot (Fig. 1d) and immunofluorescence staining (Fig. 1e) verified proper size, expression and nuclear localization of each protein.

To test our system, we targeted enhanced green fluorescent protein (eGFP; henceforth 'GFP') mRNA in a GFP-expressing HEK293T cell line. Seven plasmids individually expressing Csm1-5, Cas6 and either a GFP-targeting or nontargeting crRNA from a U6 promoter were cotransfected into cells, and GFP fluorescence assayed by flow cytometry 48 h post transfection (Supplementary Fig. 1a). Note that this strategy does not allow any means to select cells into which all plasmids were successfully delivered and will thus under-report KD efficiency. GFP KD was calculated by dividing the mean fluorescence intensity (MFI) of cells transfected with the GFP-targeting crRNA by that of cells transfected with the nontargeting crRNA (Supplementary Fig. 1b). Approximately 25% KD was observed using any of three crRNAs targeting different regions of the GFP ORF (Fig. 1f). Notably, no KD was seen after transfecting the GFP-targeting crRNA and its processing factor (Cas6) alone (Fig. 1g), indicating that KD was not due to an antisense RNA effect. Furthermore, whereas ablating DNase (H15A, D15A) or cA synthase (D577A, D578A) activities in Csm1 did not noticeably affect GFP KD, ablating RNase activity (D33A) in Csm3 abolished it (Fig. 1g), indicating RNase activity is responsible for the observed KD.

Next, we examined crRNA parameters. Naturally occurring spacers for *Sth*Csm crRNAs range from ~30 to 45 nt in length, although in vitro, spacers as short as 27 nt are sufficient to trigger all three catalytic activities[42]. We varied the GFP-targeting spacer length from 24 nt to 48 nt in increments of four and assayed GFP KD. A length of 32 nt yielded the highest KD for the crRNA tested (Fig. 1h), with little to no KD seen for lengths ≤28 nt, and diminishing KD seen for lengths ≥36 nt. A more large-scale analysis must be performed to determine whether optimal spacer length differs from sequence to sequence. Next, we examined the potential to multiplex crRNAs against several targets. We encoded two crRNAs within a single array—one targeting GFP and the other targeting mCherry (henceforth 'red fluorescent protein (RFP)')—and examined KD of GFP and RFP in a HEK293T cell line expressing both (Fig. 1i). Approximately 25% KD was achieved for both GFP and RFP regardless of the order of crRNAs in the array (GFP–RFP

Fig. 1 | An all-in-one type III CRISPR-Cas system in human cells. a, Diagram showing *cis*- and *trans*-cleavage of Cas13. **b**, Diagram showing *S. thermophilus* type III-A CRISPR-Cas locus. crRNAs are transcribed from the CRISPR array, processed by Cas6 and assemble with Csm proteins. **c**, Close-up of crRNA:target binding, showing the 6-nt cleavage pattern. **d**, Western blot showing proper size and expression of Cas/Csm proteins (red) in HEK293T cells. Csm1 and Csm4 are less stable when expressed separately[72]. GAPDH (glyceraldehyde-3-phosphate dehydrogenase) shown as loading control (green). Arrows indicate faint bands. L, ladder; U, untransfected. One of two replicates with similar results is shown. **e**, Immunofluorescence showing expression and nuclear localization of Cas/Csm proteins in HEK293T cells. Scale bar, 10 µm. One of two replicates with similar results is shown. **f**, Relative GFP fluorescence (= MFI targeting crRNA/MFI nontargeting crRNA) of HEK293T-GFP cells transfected with plasmids expressing Cas6, Csm1-5 and the indicated GFP-targeting crRNA, measured by flow cytometry. Error bars indicate mean ± s.d. of three biological replicates. **g**, Same as **f**, but with the indicated Csm mutants (or crRNA + Cas6 only). GFP crRNA 1 was used to target GFP. Error bars indicate mean ± s.d. of three biological replicates. **h**, Same as **f**, but with GFP crRNA 1 adjusted to the indicated spacer length. Error bars indicate mean ± s.d. of three biological replicates. **i**, Relative GFP and RFP fluorescence of HEK293T-GFP/RFP cells transfected with plasmids expressing Cas6, Csm1-5 and the indicated crRNAs (individual or multiplexed), measured by flow cytometry. GFP crRNA 1 was used to target GFP. RFP-targeting crRNA is listed in Supplementary Table 1. Error bars indicate mean ± s.d. of three biological replicates. **j**, Diagram showing all-in-one delivery vector designs. **k**, Western blot showing proper size and expression of Cas/Csm proteins (red) in HEK293T cells. GAPDH is shown as loading control (green). Arrows indicate each subunit. One of two replicates with similar results is shown. **l**, Relative GFP fluorescence of HEK293T-GFP cells transfected with the indicated delivery vectors and expressing the indicated GFP-targeting crRNAs, measured by flow cytometry. Error bars indicate mean ± s.d. of three biological replicates.

https://doi.org/10.1038/s41587-022-01649-9

or RFP–GFP), comparable to KD efficiency when targeting GFP or RFP alone. Together, these results demonstrate broad multiplexing capability for the Csm system.

With the Csm system up and running, we sought to simplify its delivery by consolidating all components into a single vector. For this, we pursued the following two approaches concurrently: (1) expression of each protein from separate promoters or (2) expression of all proteins from a single bidirectional promoter separated by 2A peptides (Fig. 1j). We also included RFP in the plasmid backbone to allow identification of transfected cells and thus more accurate measurement

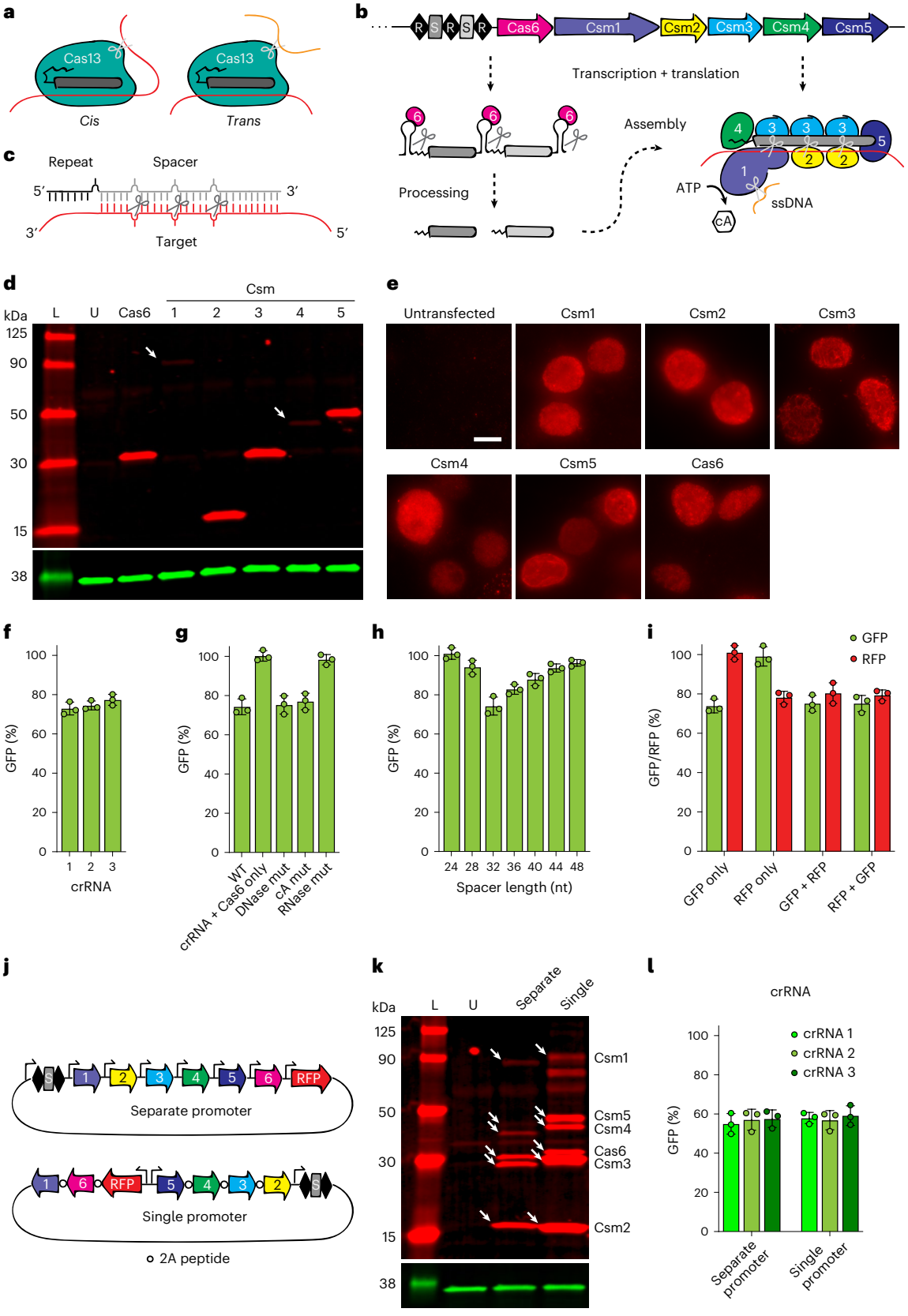

https://doi.org/10.1038/s41587-022-01649-9

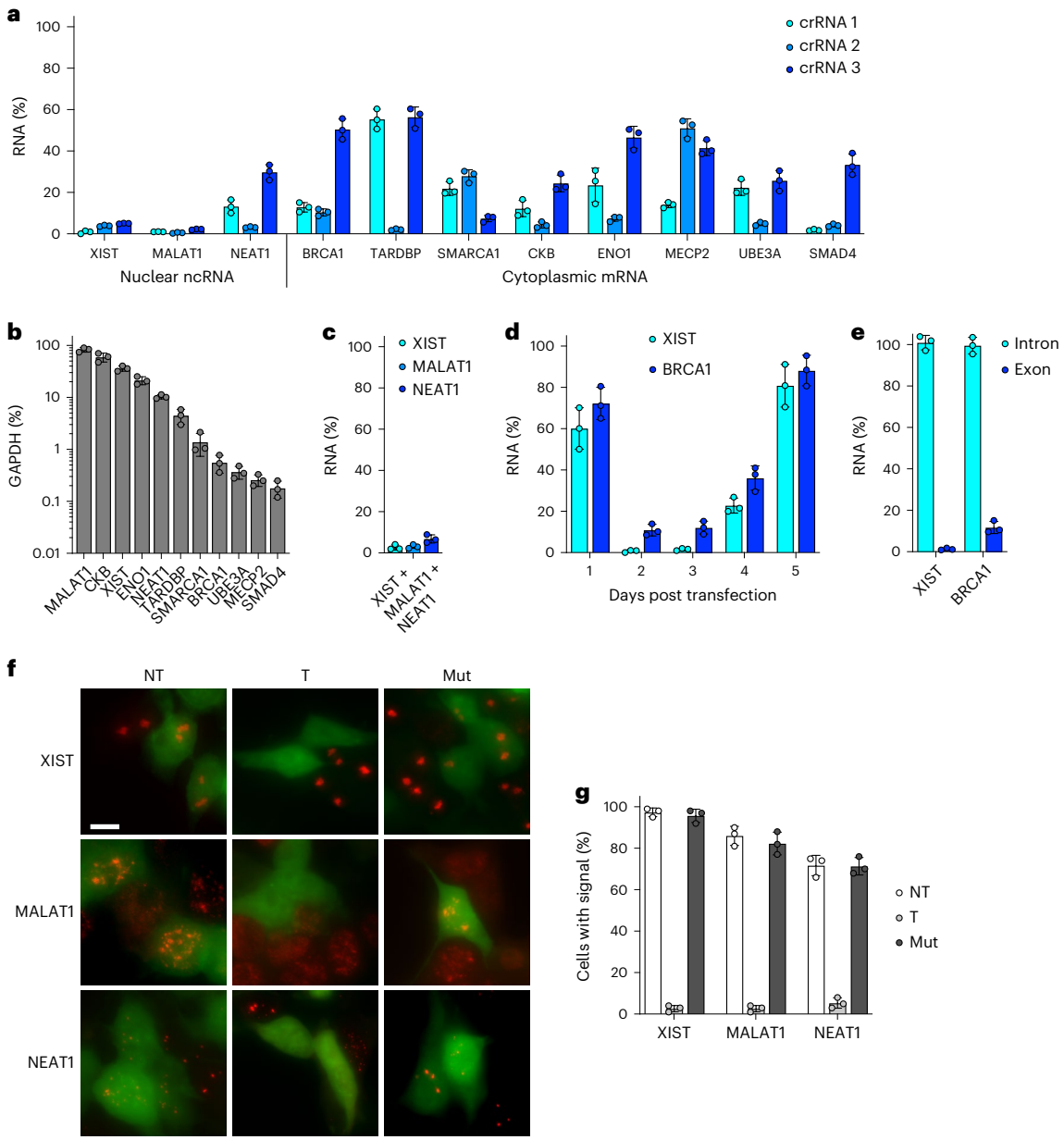

Fig. 2 | Robust KD of endogenous nuclear and cytoplasmic RNAs. a, Relative RNA abundance (normalized to nontargeting crRNA) of the indicated targets in HEK293T cells transfected with all-in-one plasmid expressing Cas/Csm proteins and the indicated crRNAs, measured by RT-qPCR. Error bars indicate mean ± s.d. of three biological replicates. **b**, Relative RNA abundance (normalized to GAPDH) of the indicated targets in untransfected HEK293T cells, measured by RT-qPCR. Error bars indicate mean ± s.d. of three biological replicates. **c**, Relative RNA abundance (normalized to nontargeting crRNA) of the indicated targets in HEK293T cells transfected with all-in-one plasmid expressing Cas/Csm proteins and the indicated crRNAs (multiplexed), measured by RT-qPCR. XIST crRNA 1, MALAT1 crRNA 1 and NEAT1 crRNA 2 were used to target XIST, MALAT1 and NEAT1, respectively. Error bars indicate mean ± s.d. of three biological replicates. **d**, Relative RNA abundance (normalized to nontargeting crRNA) of XIST and BRCA1 in HEK293T cells at the indicated times post transfection with all-in-one plasmid, measured by RT-qPCR. XIST crRNA 1 and BRCA1 crRNA 2 were used to target XIST and BRCA1, respectively. Error bars indicate mean ± s.d. of three biological replicates. **e**, Relative RNA abundance (normalized to nontargeting crRNA) of XIST and BRCA1 in HEK293T cells transfected with all-in-one plasmid expressing Cas/Csm proteins and intron- or exon-targeting crRNAs, measured by RT-qPCR. XIST crRNA 1 and BRCA1 crRNA 2 were used to target XIST and BRCA1 exons, respectively. Intron-targeting crRNAs are listed in Supplementary Table 1. Error bars indicate mean ± s.d. of three biological replicates. **f**, RNA FISH (red) for the indicated targets in HEK293T cells transfected with all-in-one plasmid expressing targeting (T) or nontargeting (NT) crRNA and RNase-active or -inactive (Mut) Cas/Csm proteins. Untransfected cells serve as internal control for transfected (green) cells. XIST crRNA 1, MALAT1 crRNA 1 and NEAT1 crRNA 2 were used to target XIST, MALAT1 and NEAT1, respectively. Scale bar, 10 µm. **g**, Quantification of **f**. One hundred transfected cells were counted for each condition. Error bars indicate mean ± s.d. of three biological replicates.

of KD efficiency (Supplementary Fig. 1c). After reconfirming proper expression of all protein components by Western blot for both plasmids (Fig. 1k), we found both strategies (after optimizing the order of proteins in the single-promoter arrangement) led to ~50% GFP KD in transfected cells (Fig. 1l). In summary, the single-promoter design is well-equipped for promoter-swapping and thus use in specific cell types or other eukaryotic systems, while the modular design of the separate-promoter vector allows for easy swapping or modification of individual Csm components. All further experiments were performed using the separate-promoter vector.

Robust KD of endogenous nuclear and cytoplasmic RNAs

Thus far, we have only used Csm to KD highly overexpressed, heterologous GFP/RFP transgenes and assayed KD at the protein level (half-life >24 h[56]), which may not accurately reflect abundance at the RNA level. We thus sought to target endogenous transcripts and assay RNA KD directly. We chose to target a panel of three nuclear noncoding RNAs (XIST, MALAT1 and NEAT1) and eight cytoplasmic mRNAs (BRCA1, TARDBP, SMARCA1, CKB, ENO1, MECP2, UBE3A and SMAD4) (Fig. 2a) of varying abundances (Fig. 2b), testing three individual crRNAs for each. HEK293T cells were transfected with all-in-one vector, transfected (RFP-positive) cells were isolated by FACS after 48 h, total cell RNA was extracted and RNA KD was assayed by RT-qPCR (Supplementary Figs. 1c and 2a,c). To our surprise, we achieved >90% KD for all eleven RNAs with at least one crRNA, compared to nontargeting crRNA control (Fig. 2a). We also confirmed multiplexed KD for three of the RNAs (XIST, MALAT1 and NEAT1) (Fig. 2c). These results demonstrate Csm to be a highly robust and efficient RNA KD tool for not only cytoplasmic but also nuclear RNAs, which are typically recalcitrant to KD by conventional RNAi methods[6].

To examine KD kinetics, we repeated the above RT-qPCR experiment for two of the RNA targets (XIST and BRCA1) across a 5-d time course. KD peaked 2–3 d post transfection and waned thereafter (Fig. 2d), as might be expected from the transient transfection method used to deliver Csm into cells. We also compared KD efficiency of crRNAs targeting intronic versus exonic regions for the same two RNAs (Fig. 2e). Targeting introns did not lead to any noticeable reduction in the mature transcript, possibly because introns are excised from the pre-mRNA more rapidly than they are cleaved by Csm.

To corroborate RNA KD with an orthogonal method, we performed RNA fluorescent in situ hybridization (FISH) for all three nuclear noncoding RNAs, which are easily visualized and display characteristic morphologies. HEK293T cells were transfected with Csm plasmid carrying a GFP reporter (to identify transfected cells) and either a targeting or nontargeting crRNA and assayed by RNA FISH after 48 h (Supplementary Fig. 2b,c). XIST, MALAT1 and NEAT1 were all readily detected when delivering a nontargeting crRNA control (Fig. 2f,g). By contrast, use of a single targeting crRNA abolished all visible signals for each target RNA in transfected (GFP-positive) cells, whereas signal was still detected in untransfected (GFP-negative) cells. For further validation, delivery of targeting crRNA with catalytically inactivated Csm (RNase mut) fully restored the detection of each target RNA. Thus, we demonstrate robust KD of endogenous transcripts using active Csm complexes by both molecular and microscopy-based techniques.

RNA KD with minimal off-targets or cytotoxicity

Next, we performed RNA sequencing (RNA-seq) to examine the potential off-target effects of Csm-mediated KD in cells. For comparison with other established KD technologies, RNA-seq was also performed for Cas13 (RfxCas13d) and RNAi (short hairpin RNA (shRNA))-mediated KD using crRNAs/shRNAs targeting the same complementary sequence[57–59]. KD was performed for 48 h, after which transfected cells were enriched by FACS and sequenced (Supplementary Fig. 3a). Scatterplots comparing transcript levels between nontargeting crRNA and empty vector (EV) control samples for Csm revealed few upregulated or downregulated transcripts (defined as ≥2-fold change, indicated in red) (Supplementary Fig. 3b), suggesting Csm expression itself does not substantially perturb the cellular environment. When targeting CKB, MALAT1, SMARCA1 or XIST, Csm-mediated KD led to significant depletion of the target transcript with few other altered transcripts (Fig. 3a,b and Supplementary Fig. 3c,d). Meanwhile, Cas13 samples showed significant KD of the target transcript while also affecting hundreds of nontarget transcripts. shRNA samples showed variable KD depending on whether the target was cytoplasmic (CKB, SMARCA1) or nuclear (MALAT1, XIST), with an intermediate amount of altered nontarget transcripts. Similar trends were seen for all four targets (Fig. 3c). Examination of RNA-seq read coverage across the target confirmed depletion was transcript-wide and not only localized near the site of Csm cleavage (red arrow), likely due to cellular exonucleotic degradation pathways[60,61] (Fig. 3d,e and Supplementary Fig 3e,f). We also examined whether Csm-mediated RNA-targeting induces any collateral changes at the DNA level due to its separate DNase activity. DNA-sequencing across the entire *CKB* locus did not reveal any noticeable differences between targeting and nontargeting samples at a sequencing depth of ~1 million reads (Supplementary Fig. 3g). Alternatively, DNase activity can be removed without affecting RNase activity (Fig. 1g)[53]. Hence, Csm-mediated RNA KD shows minimal off-target effects in human cells.

Other RNA-targeting CRISPR-Cas systems such as Cas13 suffer from severe cytotoxic effects due to inherent *trans*-cleavage activity[31–35]. Type III systems do not exhibit *trans*-activity[40] and are thus poised to offer robust RNA KD without toxicity. To check this, we tracked cell proliferation/viability using the WST-1 assay across a time course after transfecting cells with targeting or nontargeting Csm, Cas13 or shRNA constructs (Fig. 3f). Whereas cells that received targeting Cas13 constructs exhibited a significant decrease in proliferation/viability, those that received Csm or shRNA constructs were unaffected. This decrease in proliferation/viability by WST-1 assay was also seen by a more rapid decrease over time in the proportion of RFP-positive (transfected) cells within the targeting Cas13-treated population compared to the Csm- or shRNA-treated population (Fig. 3g). Taken together, these results suggest that, unlike Cas13, Csm-mediated KD has minimal toxicity in cells.

Live-cell RNA imaging without genetic manipulation

Tracking RNA in live cells remains a difficult task, often requiring genetic insertion of aptamer sequences into the target, which is both laborious and potentially disruptive to RNA function and/or regulation[62]. Fluorescently tagged programmable RNA-binding proteins such as catalytically inactivated Cas13 have recently been adopted for such purposes[17,63,64]. We asked whether the Csm complex could similarly be used to track RNA targets in live cells. To test this, we fused GFP to catalytically inactivated Csm3 (Fig. 4a), the most abundant Csm subunit (≥3 per complex), thereby allowing multivalent display. To visualize XIST RNA, we targeted a repetitive region with a single crRNA predicted to bind eight times per transcript, allowing increased signal. HEK293T cells were transfected with Csm-GFP plasmid and assayed by live-cell fluorescence microscopy after 48 h (Supplementary Fig. 4a). Whereas a nontargeting control crRNA led to only background nuclear fluorescence, the XIST-targeting crRNA led to a strong cloud-like signal in most cells (Fig. 4b,c), phenocopying what we previously observed by XIST RNA FISH (Fig. 2f). Using the same approach, we were able to visualize MALAT1 and NEAT1 transcripts, even with crRNAs predicted to bind only once per target (Fig. 4b,c). Multiplexing several crRNAs against the same target may further improve signal over background, especially for lower abundance transcripts. Thus, fluorescently tagged Csm can be used for easy visualization of RNA in living cells.

Discussion

Here we have shown that the type III-A Csm complex from *S. thermophilus* is a powerful tool for eukaryotic RNA KD. Both nuclear noncoding RNAs and cytoplasmic mRNAs were able to be knocked down with high efficiency (90–99%) and specificity (~10-fold fewer off-targets than Cas13), outperforming competing RNA KD technologies. More notably, KD was not accompanied by detectable cytotoxicity, unlike Cas13-based methods that suffer from inherent *trans*-cleavage activity[31–33,35].

Recently, *St*Csm was shown to be effective at depleting GFP or viral RNA upon delivery of bacterially purified RNP into zebrafish embryos or human cells, respectively[53,54]. While demonstrating proof of principle, RNP delivery of multisubunit CRISPR-Cas effectors is not ideal for several reasons as follows: (1) it is often difficult and short-lived

https://doi.org/10.1038/s41587-022-01649-9

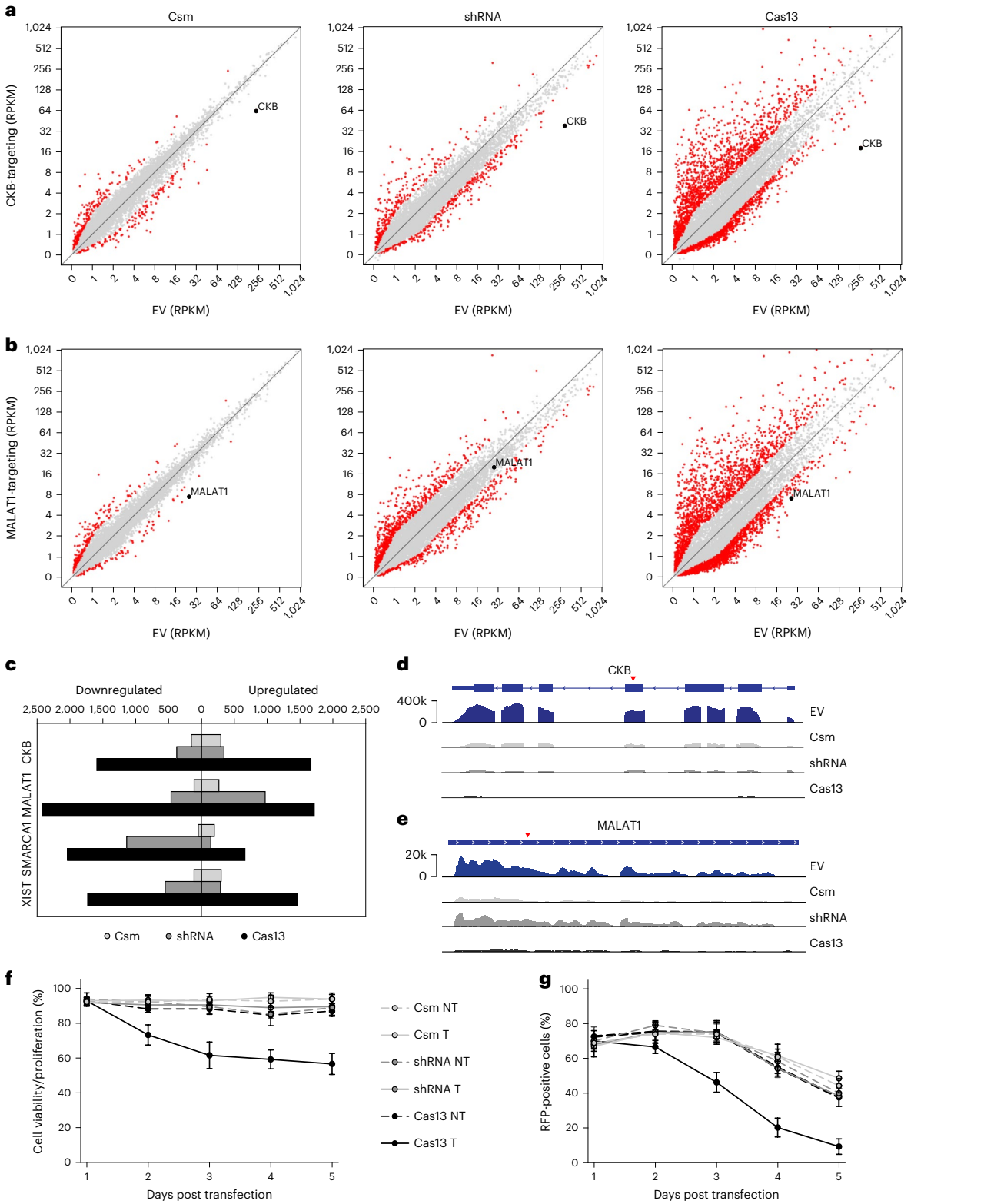

Fig. 3 | RNA KD with minimal off-targets or cytotoxicity. a,**b**, Scatterplots showing differential transcript levels between HEK293T cells transfected with plasmid expressing Csm, Cas13 or shRNA targeting CKB (**a**) or MALAT1 (**b**) versus EV control. Target transcript indicated in black; off-targets (≥2-fold change) indicated in red. **c**, Quantification of upregulated or downregulated transcripts (≥2-fold change) for each sample. CKB crRNA 1, MALAT1 crRNA 2, SMARCA1 crRNA 1 and XIST crRNA 1 were used to target CKB, MALAT1, SMARCA1 and XIST, respectively. **d**,**e**, RNA-seq read coverage across target transcripts CKB (**d**) or MALAT1 (**e**). Red arrow indicates location of crRNA/shRNA target site. **f**, Relative cell viability and proliferation (normalized to EV control) of HEK293T cells at the indicated times post transfection with the indicated targeting (T) or nontargeting (NT) plasmids, measured by WST-1 assay. CKB crRNA 1 was used for targeting. Error bars indicate mean ± s.d. of three biological replicates. **g**, Relative abundance of RFP-positive (transfected) HEK293T cells at the indicated times post transfection with the indicated targeting (T) or nontargeting (NT) plasmids, measured by flow cytometry. CKB crRNA 1 was used for targeting. Error bars indicate mean ± s.d. of three biological replicates.

https://doi.org/10.1038/s41587-022-01649-9

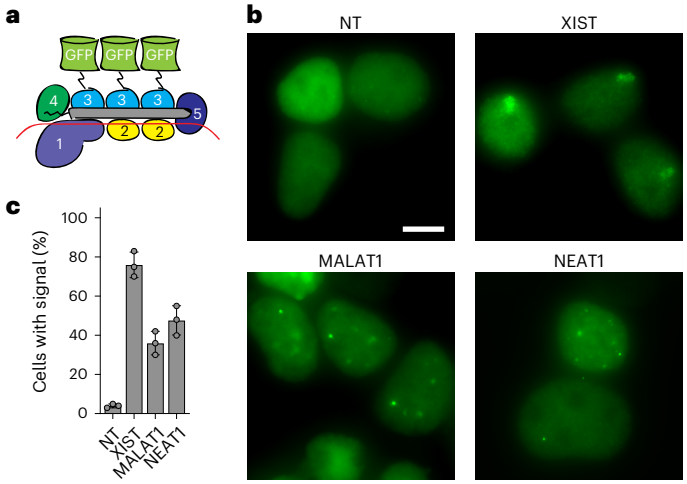

Fig. 4 | Live-cell RNA imaging without genetic manipulation. a, Diagram showing Csm3-GFP fusion complex used for live-cell imaging. **b**, Live-cell fluorescence imaging of HEK293T cells transfected with plasmid expressing Csm3-GFP fusion complex and the indicated crRNAs (Supplementary Table 1). NT, nontargeting. Scale bar, 10 µm. **c**, Quantification of **b**. One hundred transfected cells were counted for each condition. Error bars indicate mean ± s.d. of three biological replicates.

compared to DNA-delivery methods, (2) the RNP may be unstable and prone to disassembly and (3) for every new crRNA, the entire RNP must be repurified from bacteria or reconstituted from individually purified subunits in the proper ratio. We have overcome these hurdles of multicomponent CRISPR-Cas systems by encoding all necessary parts in a single deliverable plasmid.

More recently, a single-protein type III effector, Cas7–11, was characterized and used for RNA KD in eukaryotes[32]. This effector is interesting from an evolutionary and structural standpoint in that it appears to have arisen from fusion of the canonical type III subunits into one large polypeptide. While simpler to introduce into eukaryotes, Cas7–11's demonstrated RNA KD efficiency was only 25–75% for most targets (without enriching for transfected cells), making it somewhat less practical as a tool. Meanwhile, two new reports of naturally occurring and engineered high-fidelity Cas13 variants claim to have mitigated *trans*-cleavage activity (and thus cytotoxicity) while preserving on-target activity[35,57]—although a mechanistic explanation for this remains unclear. Cas7–11 and high-fidelity Cas13s await further characterization before widespread use.

A key advantage of our approach over RNAi is the ability to target transcripts in the nucleus. We were able to achieve >95% KD for three biologically significant nuclear ncRNAs (XIST, MALAT1 and NEAT1). Nuclear RNAs are notoriously difficult to KD, often requiring expensive chemically modified antisense oligos to direct RNase H-mediated cleavage[6]. However, the increased stability of these oligos often leads to unexpected off-target hybridization and cytotoxic effects. Aside from long ncRNAs, nuclear targeting may prove useful for the study of other ncRNA species such as eRNAs, tRNAs, rRNAs, circRNAs, miRNAs and snoRNAs. For instance, it will be interesting to see whether targeting introns containing miRNA or snoRNA clusters enables their degradation before processing/maturation, or whether targeting particular exons alters the abundance of mRNA splice isoforms.

Another advantage of our system is its ease of multiplexing. Multiple spacers can be cloned into the CRISPR array and processed into individual crRNAs by Cas6. This allows for pooled screening, either by encoding crRNAs against multiple targets at once or encoding multiple crRNAs against the same target. The latter may enable robust KD on the first try without the need to individually screen multiple crRNAs against a target. An unexpected observation was the titratable nature of KD with increasing spacer length. This may allow for easy tunability of KD (rather than all-or-none) when studying concentration-dependent effects of gene products.

Csm-mediated RNA KD appears to be robust. We were able to achieve significant KD for nearly all targets tested, with at least one of three crRNAs per target yielding >90% KD. Because, like other RNA-targeting CRISPR-Cas systems, Csm does not have any PAM requirement for target site selection, the only criteria we used were that the target be a unique sequence in the human transcriptome and the spacer avoid stretches of ≥5 consecutive Ts, which might cause premature Pol III transcriptional termination within the crRNA sequence[65]. The observed variability in KD efficiency from one crRNA to another may in part be explained by differences in target site accessibility due to local RNA secondary structure or protein occupancy[66]. A more large-scale analysis must be performed to determine optimal spacer design criteria, and to test how different factors (for example, melting temperature, GC content and target site availability) influence KD efficiency.

We showed that fluorescently tagged, catalytically inactivated Csm can be used for live-cell RNA visualization. By fusing GFP to the most abundant subunit (Csm3), we were able to achieve multivalent display (≥3x GFP per complex), which may offer unique advantages over single-subunit effectors such as Cas13. Beyond GFP, other proteins of interest may be fused to the various Csm subunits to achieve assembly or tethering at a desired stoichiometric ratio. Thus, as a multisubunit complex, Csm offers the benefits of split-protein systems without the engineering effort. Catalytically inactivated Csm might also be useful for disrupting RNA structural motifs or RNA-protein interactions without manipulation at the DNA level.

Finally, this work utilized only the RNase activity of Csm while ignoring its DNase and cA synthase activities. In prokaryotes, cA signaling appears to be the main defensive strategy employed by type III systems[67], leading to the activation of various downstream effectors[50,51]. These effectors range from RNases to DNases, proteases and transcription factors[68–71]. cA molecules and reliant pathways are currently not known to exist in eukaryotes and thus could be introduced in an orthogonal manner. By bringing type III systems to eukaryotes, we have paved the way for co-introduction of related *trans*-effectors that can be activated in an RNA sequence-dependent manner (Supplementary Fig. 4b). This has important implications for the development of RNA diagnostics, screens and synthetic circuits in vivo.

Online content

Any methods, additional references, Nature Portfolio reporting summaries, source data, extended data, supplementary information, acknowledgements, peer review information; details of author contributions and competing interests; and statements of data and code availability are available at https://doi.org/10.1038/s41587-022-01649-9.

References

1. Wilson, R. C. & Doudna, J. A. Molecular mechanisms of RNA interference. *Annu. Rev. Biophys.* **42**, 217–239 (2013).
2. Carthew, R. W. & Sontheimer, E. J. Origins and mechanisms of miRNAs and siRNAs. *Cell.* **136**, 642–655 (2009).
3. Jackson, A. L. et al. Expression profiling reveals off-target gene regulation by RNAi. *Nat. Biotechnol.* **21**, 635–637 (2003).
4. Jackson, A. L. et al. Widespread siRNA 'off-target' transcript silencing mediated by seed region sequence complementarity. *RNA* **12**, 1179–1187 (2006).
5. Birmingham, A. et al. 3′ UTR seed matches, but not overall identity, are associated with RNAi off-targets. *Nat. Methods* **3**, 199–204 (2006).
6. Behlke, M. Mini-review on current strategies to knockdown long non-coding RNAs. *J. Rare Dis. Res. Treat.* **1**, 66–70 (2016).

7. Zeng, Y. & Cullen, B. R. RNA interference in human cells is restricted to the cytoplasm. *RNA* **8**, 855–860 (2002).
8. Aravind, L., Watanabe, H., Lipman, D. J. & Koonin, E. V. Lineage-specific loss and divergence of functionally linked genes in eukaryotes. *Proc. Natl Acad. Sci. USA* **97**, 11319–11324 (2000).
9. Nakayashiki, H., Kadotani, N. & Mayama, S. Evolution and diversification of RNA silencing proteins in fungi. *J. Mol. Evol.* **63**, 127–135 (2006).
10. Zhao, Z., Cao, Y., Li, M. & Meng, A. Double-stranded RNA injection produces nonspecific defects in zebrafish. *Dev. Biol.* **229**, 215–223 (2001).
11. Oates, A. C., Bruce, A. E. & Ho, R. K. Too much interference: injection of double-stranded RNA has nonspecific effects in the zebrafish embryo. *Dev. Biol.* **224**, 20–28 (2000).
12. Barrangou, R. et al. CRISPR provides acquired resistance against viruses in prokaryotes. *Science* **315**, 1709–1712 (2007).
13. Brouns, S. J. J. et al. Small CRISPR RNAs guide antiviral defense in prokaryotes. *Science* **321**, 960–964 (2008).
14. Jinek, M. et al. A programmable dual-RNA-guided DNA endonuclease in adaptive bacterial immunity. *Science* **337**, 816–821 (2012).
15. Cong, L. et al. Multiplex genome engineering using CRISPR/Cas systems. *Science* **339**, 819–823 (2013).
16. Mali, P. et al. RNA-guided human genome engineering via Cas9. *Science* **339**, 823–826 (2013).
17. Abudayyeh, O. O. et al. RNA targeting with CRISPR-Cas13. *Nature* **550**, 280–284 (2017).
18. Abudayyeh, O. O. et al. C2c2 is a single-component programmable RNA-guided RNA-targeting CRISPR effector. *Science* **353**, aaf5573 (2016).
19. Konermann, S. et al. Transcriptome engineering with RNA-targeting type VI-D CRISPR effectors. *Cell* **173**, 665–676 (2018).
20. Song, J.-J., Smith, S. K., Hannon, G. J. & Joshua-Tor, L. Crystal structure of Argonaute and its implications for RISC slicer activity. *Science* **305**, 1434–1437 (2004).
21. East-Seletsky, A. et al. Two distinct RNase activities of CRISPR-C2c2 enable guide-RNA processing and RNA detection. *Nature* **538**, 270–273 (2016).
22. Zhang, C. et al. Structural basis for the RNA-guided ribonuclease activity of CRISPR-Cas13d. *Cell* **175**, 212–223 (2018).
23. Slaymaker, I. M. et al. High-resolution structure of Cas13b and biochemical characterization of RNA targeting and cleavage. *Cell Rep.* **26**, 3741–3751 (2019).
24. Liu, L. et al. The molecular architecture for RNA-guided RNA cleavage by Cas13a. *Cell* **170**, 714–726 (2017).
25. Liu, L. et al. Two distant catalytic sites are responsible for C2c2 RNase activities. *Cell* **168**, 121–134 (2017).
26. Gootenberg, J. S. et al. Nucleic acid detection with CRISPR-Cas13a/C2c2. *Science* **356**, 438–442 (2017).
27. Gootenberg, J. S. et al. Multiplexed and portable nucleic acid detection platform with Cas13, Cas12a, and Csm6. *Science* **360**, 439–444 (2018).
28. Liu, T. Y. et al. Accelerated RNA detection using tandem CRISPR nucleases. *Nat. Chem. Biol.* **17**, 982–988 (2021).
29. Fozouni, P. et al. Amplification-free detection of SARS-CoV-2 with CRISPR-Cas13a and mobile phone microscopy. *Cell* **184**, 323–333 (2021).
30. Meeske, A. J., Nakandakari-Higa, S. & Marraffini, L. A. Cas13-induced cellular dormancy prevents the rise of CRISPR-resistant bacteriophage. *Nature* **570**, 241–245 (2019).
31. Wang, Q. et al. The CRISPR-Cas13a gene-editing system induces collateral cleavage of RNA in glioma cells. *Adv. Sci.* **6**, 1901299 (2019).
32. Özcan, A. et al. Programmable RNA targeting with the single-protein CRISPR effector Cas7–11. *Nature* **597**, 720–725 (2021).
33. Ai, Y., Liang, D. & Wilusz, J.E. CRISPR/Cas13 effectors have differing extents of off-target effects that limit their utility in eukaryotic cells. *Nucleic Acids Res.* **50**, e65 (2022).
34. Shi, P., et al. RNA-guided cell targeting with CRISPR/RfxCas13d collateral activity in human cells. Preprint at *bioRxiv* https://doi.org/10.1101/2021.11.30.470032 (2021).
35. Tong, H. et al. High-fidelity Cas13 variants for targeted RNA degradation with minimal collateral effects. *Nat. Biotechnol.* https://doi.org/10.1038/s41587-022-01419-7 (2022).
36. Makarova, K. S. et al. An updated evolutionary classification of CRISPR-Cas systems. *Nat. Rev. Microbiol.* **13**, 722–736 (2015).
37. Pickar-Oliver, A. et al. Targeted transcriptional modulation with type I CRISPR-Cas systems in human cells. *Nat. Biotechnol.* **37**, 1493–1501 (2019).
38. Cameron, P. et al. Harnessing type I CRISPR-Cas systems for genome engineering in human cells. *Nat. Biotechnol.* **37**, 1471–1477 (2019).
39. Chen, Y. et al. Repurposing type I-F CRISPR-Cas system as a transcriptional activation tool in human cells. *Nat. Commun.* **11**, 3136 (2020).
40. Staals, R. H. J. et al. RNA targeting by the type 3-A CRISPR-Cas Csm complex of Thermus thermophilus. *Mol. Cell* **56**, 518–530 (2014).
41. Zhu, Y., Klompe, S.E., Vlot, M., van der Oost, J. & Staals, R.H.J. Shooting the messenger: RNA-targetting CRISPR-Cas systems. *Biosci. Rep.* **28**, BSR20170788 (2018).
42. You, L. et al. Structure studies of the CRISPR-Csm complex reveal mechanism of co-transcriptional interference. *Cell* **176**, 239–253 (2019).
43. Tamulaitis, G. et al. Programmable RNA shredding by the type 3-A CRISPR-Cas system of Streptococcus thermophilus. *Mol. Cell* **56**, 506–517 (2014).
44. Jia, N. et al. Type 3-A CRISPR-Cas csm complexes: assembly, periodic RNA cleavage, DNase activity regulation, and autoimmunity. *Mol. Cell* **73**, 264–277 (2019).
45. Guo, M. et al. Coupling of ssRNA cleavage with DNase activity in type 3-A CRISPR-Csm revealed by cryo-EM and biochemistry. *Cell Res.* **29**, 305–312 (2019).
46. Liu, T. Y., Iavarone, A. T. & Doudna, J. A. RNA and DNA targeting by a reconstituted Thermus thermophilus Type 3-A CRISPR-Cas system. *PLoS ONE* **12**, e0170552 (2017).
47. Mogila, I. et al. Genetic dissection of the type 3-A CRISPR-Cas system Csm complex reveals roles of individual subunits. *Cell Rep.* **26**, 2753–2765 (2019).
48. Kazlauskiene, M., Tamulaitis, G., Kostiuk, G., Venclovas, Č. & Siksnys, V. Spatiotemporal control of type 3-A CRISPR-Cas immunity: coupling DNA degradation with the target RNA recognition. *Mol. Cell* **62**, 295–306 (2016).
49. Samai, P. et al. Co-transcriptional DNA and RNA cleavage during type 3 CRISPR-Cas immunity. *Cell* **161**, 1164–1174 (2015).
50. Niewoehner, O. et al. Type 3 CRISPR-Cas systems produce cyclic oligoadenylate second messengers. *Nature* **548**, 543–548 (2017).
51. Kazlauskiene, M., Kostiuk, G., Venclovas, Č., Tamulaitis, G. & Siksnys, V. A cyclic oligonucleotide signaling pathway in type 3 CRISPR-Cas systems. *Science* **357**, 605–609 (2017).
52. Wang, B. et al. Structural basis for self-cleavage prevention by tag:anti-tag pairing complementarity in type VI Cas13 CRISPR systems. *Mol. Cell* **81**, 1100–1115 (2021).
53. Fricke, T. et al. Targeted RNA knockdown by a type 3 CRISPR-Cas complex in zebrafish. *CRISPR J.* **3**, 299–313 (2020).

54. Lin, P. et al. Type 3 CRISPR-based RNA editing for programmable control of SARS-CoV-2 and human coronaviruses. *Nucleic Acids Res.* **50**, e47 (2022).
55. Staals, R. H. J. et al. Structure and activity of the RNA-targeting Type 3-B CRISPR-Cas complex of Thermus thermophilus. *Mol. Cell* **52**, 135–145 (2013).
56. Corish, P. & Tyler-Smith, C. Attenuation of green fluorescent protein half-life in mammalian cells. *Protein Eng.* **12**, 1035–1040 (1999).
57. Wei, J., et al. Deep learning of Cas13 guide activity from high-throughput gene essentiality screening. Preprint at *bioRxiv* https://doi.org/10.1101/2021.09.14.460134 (2021).
58. Bofill-De Ros, X. & Gu, S. Guidelines for the optimal design of miRNA-based shRNAs. *Methods* **103**, 157–166 (2016).
59. Wessels, H.-H. et al. Massively parallel Cas13 screens reveal principles for guide RNA design. *Nat. Biotechnol.* **38**, 722–727 (2020).
60. Houseley, J. & Tollervey, D. The many pathways of RNA degradation. *Cell* **136**, 763–776 (2009).
61. Lima, W. F., De Hoyos, C. L., Liang, X.-H. & Crooke, S. T. RNA cleavage products generated by antisense oligonucleotides and siRNAs are processed by the RNA surveillance machinery. *Nucleic Acids Res.* **44**, 3351–3363 (2016).
62. George, L., Indig, F. E., Abdelmohsen, K. & Gorospe, M. Intracellular RNA-tracking methods. *Open Biol.* **8**, 180104 (2018).
63. Wang, H. et al. CRISPR-mediated live imaging of genome editing and transcription. *Science* **365**, 1301–1305 (2019).
64. Yang, L.-Z. et al. Dynamic imaging of RNA in living cells by CRISPR-Cas13 systems. *Mol. Cell* **76**, 981–997 (2019).
65. Gao, Z., Herrera-Carrillo, E. & Berkhout, B. Delineation of the exact transcription termination signal for type 3 polymerase 3. *Mol. Ther. Nucleic Acids* **10**, 36–44 (2018).
66. Grüschow, S., Adamson, C. S. & White, M. F. Specificity and sensitivity of an RNA targeting type 3 CRISPR complex coupled with a NucC endonuclease effector. *Nucleic Acids Res.* **49**, 13122–13134 (2021).
67. Rostøl, J. T. & Marraffini, L. A. Non-specific degradation of transcripts promotes plasmid clearance during type 3-A CRISPR-Cas immunity. *Nat. Microbiol.* **4**, 656–662 (2019).
68. Huang, F. & Zhu, B. The cyclic oligoadenylate signaling pathway of type 3 CRISPR-Cas systems. *Front. Microbiol.* **11**, 602789 (2020).
69. Makarova, K. S. et al. Evolutionary and functional classification of the CARF domain superfamily, key sensors in prokaryotic antivirus defense. *Nucleic Acids Res.* **48**, 8828–8847 (2020).
70. Athukoralage, J. S. & White, M. F. Cyclic oligoadenylate signalling and regulation by ring nucleases during type 3 CRISPR defence. *RNA* **27**, 855–867 (2021).
71. Rouillon, C., et al. SAVED by a toxin: structure and function of the CRISPR Lon protease. Preprint at *bioRxiv* https://doi.org/10.1101/2021.12.06.471393 (2021).
72. Park, K.-H. et al. RNA activation-independent DNA targeting of the Type 3 CRISPR-Cas system by a Csm complex. *EMBO Rep.* **18**, 826–840 (2017).

Methods

Cell lines and culture conditions

HEK293T, HEK293T-GFP and HEK293T-GFP/RFP cells (UC Berkeley Cell Culture Facility) were grown in medium containing DMEM, high glucose, GlutaMAX supplement, sodium pyruvate (Thermo Fisher Scientific), 10% FBS (Sigma), 25 mM HEPES pH 7.2–7.5 (Thermo Fisher Scientific), 1× MEM nonessential amino acids (Thermo Fisher Scientific), 1× Pen/Strep (Thermo Fisher Scientific) and 0.1 mM βME (Thermo Fisher Scientific) at 37 °C with 5% CO_2. All cell lines were verified to be mycoplasma-free (abm, PCR mycoplasma detection kit).

Plasmid construction and cloning

CRISPR-Cas/Csm sequences were derived from *S. thermophilus* strain ND03 (NCBI). Protein sequences were human codon optimized using online tools (GenScript), synthesized as gene blocks (IDT), modified using PCR and cloned into custom eukaryotic expression vectors (derived from pUC19) by Golden Gate assembly, Gibson assembly (NEB), or Gibson assembly Ultra (Synthetic Genomics). Plasmids were verified by Sanger or whole-plasmid sequencing. All cloning was performed in Stbl3 *Escherichia coli* (Thermo Fisher Scientific) to prevent recombination between repetitive sequences. crRNA/shRNA sequences are provided in Supplementary Table 1. Plasmid sequences are provided in Supplementary Table 2.

DNA transfections

According to the manufacturer's instructions, 1×10^6 HEK293T cells were transfected with 2.5 µg plasmid DNA using 7.5 µl FuGENE HD transfection reagent in 6-well plates. Following transfection, cells were grown for 48 h to allow plasmid expression and RNA KD to occur, unless otherwise stated.

Flow cytometry

Cell fluorescence was assayed on an Attune NxT acoustic focusing cytometer (Thermo Fisher Scientific) equipped with 488 nm excitation laser and 530/30 emission filter (eGFP), and 561 nm excitation laser and 620/15 emission filter (mCherry). Data were analyzed using Attune Cytometric Software v5.1.1 and FlowJo v10.7.1.

FACS

Cells were sorted by fluorescence on a Sony Cell Sorter SH800Z (100 µm sorting chip) equipped with 488 nm excitation laser and 525/50 emission filter (eGFP), and 561 nm excitation laser and 600/60 emission filter (mCherry). Data were analyzed using Sony Cell Sorter Software v2.1.5.

RT-qPCR

Total cell RNA was extracted using TRIzol Reagent (Thermo Fisher Scientific) as per the manufacturer's instructions. Genomic DNA was removed using TURBO DNase (Thermo Fisher Scientific). After inactivating TURBO DNase with DNase Inactivating Reagent, 1 µg DNase-free RNA was reverse transcribed using SuperScript III Reverse Transcriptase (Thermo Fisher Scientific) with random primers (Promega) as per manufacturer's instructions. qPCR was performed using iTaq Universal SYBR Green Supermix (Bio-Rad) in a CFX96 Real-Time PCR Detection System (Bio-Rad). Gene-specific primer pairs used to detect mature transcripts are listed in Supplementary Table 1. Relative amount of a given target RNA under targeting versus nontargeting conditions was calculated using the formula $2^{-((Ct_{Target}-Ct_{GAPDH})_{Targeting\ crRNA} - (Ct_{Target}-Ct_{GAPDH})_{NT\ crRNA})}$. No-RT and no-template controls were run alongside all RT-qPCR experiments.

Cell viability and proliferation assay

The WST-1 assay was used to quantify cell viability and proliferation. Cells transfected with Csm, Cas13 or shRNA plasmids were grown in 96-well plates until the indicated timepoints, incubated with WST-1 reagent (Sigma) at 37 °C for 1 h as per manufacturer's instructions, and absorbance measured using a Cytation five microplate reader (BioTek Instruments) at 450 nm with 600 nm reference.

Microscopy

For wide-field fluorescent imaging, cells were observed on a Zeiss Axio Observer Z1 inverted fluorescence microscope, equipped with 63/1.4 NA oil DIC and 100×/1.4 NA oil Ph3 Plan Apochromat objective lenses, ORCA-Flash4.0 camera (Hamamatsu) and ZEN 2012 software. Images represent max-intensity z-projections and were generated using ZEN 2012 (Zeiss) and FIJI (ImageJ) software. For live-cell imaging, cells were grown on chambered 1.5 coverglasses (Nunc Lab-Tek 2) in medium lacking phenol red (Thermo Fisher Scientific) and imaged directly on the inverted fluorescent microscope.

RNA FISH

Cells were grown on glass coverslips and rinsed in PBS. They were fixed in 4% paraformaldehyde for 10 min at room temp and then permeabilized in PBS/0.5% Triton X-100 for 10 min. Cells were dehydrated in a series of 70%, 80%, 90% and 100% ethanol for 5 min each. Labeled oligo probe pool (10 nM final) was added to hybridization buffer containing 25% formamide, 2× SSC, 10% dextran sulfate and nonspecific competitor (0.1 mg ml^{-1} human Cot-1 DNA (Thermo Fisher Scientific)). Hybridization was performed in a humidified chamber at 37 °C overnight. After being washed once in 25% formamide/2× SSC at 37 °C for 20 min and three times in 2× SSC at 37 °C for 5 min each, cells were mounted for wide-field fluorescent imaging. Nuclei were counter-stained with Hoechst 33342 (Life Technologies).

FISH probes

XIST oligo FISH probes were designed against the 'Repeat D' region of human XIST RNA and synthesized by IDT carrying a 5′ Cy3 dye modification (see Supplementary Table 1 for sequences). MALAT1 and NEAT1 oligo FISH probes were ordered from LGC Biosearch Technologies (SMF-2035-1, SMF-2036-1) carrying a Quasar 570 dye modification.

Immunofluorescence

Cells were grown on glass coverslips and rinsed in PBS. They were fixed in 4% paraformaldehyde for 10 min and then permeabilized in PBS/0.5% Triton X-100 for 10 min at room temp. Cells were blocked with blocking buffer (PBS/0.05% Tween-20 containing 1% BSA) for 1 h, incubated with primary antibody in blocking buffer for 1 h, washed three times with PBS/0.05% Tween-20 for 5 min each, incubated with dye-conjugated secondary antibody in blocking buffer for 1 h at room temp and washed three times again with PBS/0.05% Tween-20 for 5 min each. Cells were mounted for wide-field fluorescent imaging and nuclei were counter-stained with Hoechst 33342 (Life Technologies).

Western blot

Cells were washed once with PBS and lysed in cold RIPA lysis buffer (50 mM Tris pH 7.5, 150 mM NaCl, 1% NP-40, 1% sodium deoxycholate, 0.1% SDS, 1× protease inhibitor cocktail (Sigma)). Lysate was sonicated (Qsonica Q800 Sonicator) in polystyrene tubes at 50% power setting, 30 s on/30 s off for a total sonication time of 5 min at 4 °C. After removing debris by centrifugation at 16,000*g* for 10 min, protein concentration in the supernatant was measured (Pierce BCA Assay Kit). 20–50 µg protein lysate was denatured in 1× Laemmli buffer at 95 °C for 10 min and resolved by SDS-PAGE. Protein was transferred to Immun-Blot LF PVDF membrane (Bio-Rad). The membrane was blocked with blocking buffer (PBS/0.05% Tween-20 containing 5% milk) for 1 h at room temp, incubated with primary antibody in blocking buffer overnight at 4 °C, washed three times with PBS/0.05% Tween-20 for 5 min each, incubated with dye-conjugated secondary antibody in blocking buffer for 1 h at room temp and washed three times again with PBS/0.05% Tween-20 for 5 min each. Protein bands were visualized on an LI-COR Odyssey CLx with Image Studio v5.2 software using 700 nm and 800 nm channels.

Antibodies
For Western blot, the following primary antibodies were used: mice anti-FLAG (Sigma, F1804, Lot SLCC6485; 1:2,000 dilution) and rabbit anti-GAPDH (Cell Signaling Technology, 14C10, Lot 14, 1:5,000 dilution); the following secondary antibodies were used: IRDye 680RD goat antimouse (LI-COR, 926-68070, Lot C90910-21; 1:20,000 dilution), IRDye 800CW goat antirabbit (LI-COR, 926-32211, Lot C90723-19; 1:20,000 dilution). For immunofluorescence, the following primary antibodies were used: mice anti-FLAG (Sigma, F1804, Lot SLCC6485; 1:500 dilution); the following secondary antibodies were used: Alexa Fluor 555 goat antimouse (Invitrogen, A21424, Lot 2123594; 1:2,000 dilution).

DNA-seq
Cells were lysed with Laird lysis buffer (10 mM Tris pH 8, 5 mM EDTA pH 8, 200 mM NaCl, 0.2% SDS, 0.2 mg ml^{-1} proteinase K) at 55 °C for 2 h and genomic DNA extracted with phenol-chloroform. The *CKB* locus was amplified from genomic DNA by PCR (primer sequences listed in Supplementary Table 1) using PrimeSTAR GXL DNA polymerase (Takara Bio). The full-length PCR amplicon was purified from agarose gel and sheared by sonication to 200–400 bp fragments using a Qsonica Q800 Sonicator at 50% power setting, 30 s on/30 s off, for a total sonication time of 8 min at 4 °C. DNA libraries were prepared using NEBNext Ultra II DNA Library Prep Kit for Illumina, as per manufacturer's instructions. Libraries were sequenced in-house (Center for Translational Genomics, UC Berkeley) on an iSeq100 with a 150 bp paired-end run configuration to a depth of ~1 million reads each, with one biological replicate per sample.

DNA-seq analysis
Reads were aligned to the *CKB* (ENSG00000166165) gene locus with BWA MEM (v0.7.17) and PCR duplicates were removed with Picard Tools (v2.21.9). Mismatches and indels at each position were tabulated with Pysamstats (v1.1.2).

RNA-seq
Total cell RNA was extracted using TRIzol Reagent (Thermo Fisher Scientific). PolyA mRNA was isolated using NEBNext PolyA mRNA Isolation Module (NEB), as per the manufacturer's instructions. Strand-specific cDNA libraries were prepared using NEBNext Ultra II Directional RNA Library Prep Kit for Illumina, as per the manufacturer's instructions. Libraries were sequenced by Novogene, Genewiz or UCSF Center for Advanced Technology on a NovaSeq6000 with a 150 bp paired-end run configuration to a depth of ~30 million reads each, with one biological replicate per sample.

RNA-seq analysis
Reads were assessed for sequencing quality with FastQC (v0.11.9), then adapters and low-quality bases were trimmed with CutAdapt (v4.1). Samples were aligned to the GRCh38 reference genome (GENCODE Release 39) with STAR (v2.7.10a) and uniquely mapped reads were used to generate a strand-specific count matrix with featureCounts (v2.0.3). EdgeR (v3.36.0) calcNormFactors was used to normalize samples according to seven housekeeping genes (UBC, HMBS, TBP, GAPDH, HPRT1, RPL13A and ACTB) before calculating RPKM. Transcripts with a ≥2-fold change relative to EV control were considered upregulated or downregulated.

Statistical analysis
All graphs display the mean and standard deviation of three biological replicates. For RNA-seq analysis, no statistical parameters were applied given one biological replicate.

Reporting summary
Further information on research design is available in the Nature Portfolio Reporting Summary linked to this article.

Data availability
RNA-seq and DNA-seq datasets have been deposited at GEO (accession number GSE220741)[73] and SRA (accession number PRJNA911336)[74], respectively. Essential plasmids have been deposited at Addgene (plasmid ID numbers 195237–195242). Microscope image files have been deposited at figshare (https://doi.org/10.6084/m9.figshare.21714815.v1). The GRCh38 reference genome is publicly available (GENCODE Release 39). Source data are provided with this paper, including unprocessed blots.

Code availability
All codes are available upon request.

References
73. Marena, T., David, C., Jennifer, D. Transcriptome analysis of targeted RNA-knockdown using CRISPR-Csm in HEK293T cells. *NCBI* https://www.ncbi.nlm.nih.gov/geo/query/acc.cgi?acc=GSE220741 (2022).
74. Characterization of CRISPR-Csm DNAse activity during targeted RNA-knockdown in eukaryotes. *NCBI* https://www.ncbi.nlm.nih.gov/bioproject/PRJNA911336/ (2022).

Acknowledgements
We thank all members of the Doudna lab for helpful advice and discussion. We also acknowledge N. Krishnappa (Center for Translational Genomics Innovative, UC Berkeley) and E. Chow (Center for Advanced Technology, UCSF) for assistance with NGS. This project was supported by NIH/SCGE fund U01AI142817 and NSF fund 1817593. Sequencing at the UCSF CAT was supported by UCSF PBBR, RRP IMIA and NIA 1S10OD028511-01 grants. D.C. is supported by the J. Coffin Childs Memorial Fund for Medical Research. J.A.D. is an investigator at the Howard Hughes Medical Institute.

Author contributions
D.C. and J.A.D. conceived of the project. J.A.D. supervised the project. D.C. designed and performed all experiments. M.T. performed all bioinformatics analyses. D.C., M.T. and J.A.D. wrote the paper.

Competing interests
The Regents of the University of California have filed a related patent, for which D.C. and J.A.D. are inventors, on the use of the Csm system for eukaryotic RNA KD with the United States Patent and Trademark Office. J.A.D. is a cofounder of Caribou Biosciences, Editas Medicine, Intellia Therapeutics and Mammoth Biosciences, and a director of Johnson & Johnson, Altos Labs and Tempus. J.A.D. is a scientific advisor to Caribou Biosciences, Intellia Therapeutics, Mammoth Biosciences, Scribe Therapeutics, Algen, Felix and Inari; J.A.D. serves on the scientific advisory boards of Sixth Street and The Column Group. J.A.D. has research projects sponsored by Roche and Apple Tree Partners. The other author declares no competing interests.

Additional information
Supplementary information The online version contains supplementary material available at https://doi.org/10.1038/s41587-022-01649-9.

Correspondence and requests for materials should be addressed to Jennifer A. Doudna.

Peer review information *Nature Biotechnology* thanks Malcolm White and the other, anonymous, reviewer(s) for their contribution to the peer review of this work.

nature research

Corresponding author(s): Jennifer A. Doudna

Last updated by author(s): 2022/12/10

Reporting Summary

Nature Research wishes to improve the reproducibility of the work that we publish. This form provides structure for consistency and transparency in reporting. For further information on Nature Research policies, see our Editorial Policies and the Editorial Policy Checklist.

Statistics

For all statistical analyses, confirm that the following items are present in the figure legend, table legend, main text, or Methods section.

n/a	Confirmed	
☐	☒	The exact sample size (*n*) for each experimental group/condition, given as a discrete number and unit of measurement
☒	☐	A statement on whether measurements were taken from distinct samples or whether the same sample was measured repeatedly
☒	☐	The statistical test(s) used AND whether they are one- or two-sided *Only common tests should be described solely by name; describe more complex techniques in the Methods section.*
☒	☐	A description of all covariates tested
☒	☐	A description of any assumptions or corrections, such as tests of normality and adjustment for multiple comparisons
☐	☒	A full description of the statistical parameters including central tendency (e.g. means) or other basic estimates (e.g. regression coefficient) AND variation (e.g. standard deviation) or associated estimates of uncertainty (e.g. confidence intervals)
☒	☐	For null hypothesis testing, the test statistic (e.g. *F*, *t*, *r*) with confidence intervals, effect sizes, degrees of freedom and *P* value noted *Give P values as exact values whenever suitable.*
☒	☐	For Bayesian analysis, information on the choice of priors and Markov chain Monte Carlo settings
☒	☐	For hierarchical and complex designs, identification of the appropriate level for tests and full reporting of outcomes
☒	☐	Estimates of effect sizes (e.g. Cohen's *d*, Pearson's *r*), indicating how they were calculated

Our web collection on statistics for biologists contains articles on many of the points above.

Software and code

Policy information about availability of computer code

Data collection	ZEN (2012), Attune Cytometric Software (v5.1.1), Sony Cell Sorter Software (v2.1.5), Image Studio (v5.2)
Data analysis	FlowJo (v10.7.1), FIJI (ImageJ), GraphPad Prism (v9.3.1), BWA-MEM (v0.7.17), Picard Tools (v2.21.9), CutAdapt (v4.1), STAR (v2.7.10a), featureCounts (v2.0.3), EdgeR (v3.36.0), Samtools (v4.1.1), R (v4.1.1), Python (v3.9.12), Pysamstats (v1.1.2), FastQC (v0.11.9), matplotlib (v3.6.0), custom code available upon request

For manuscripts utilizing custom algorithms or software that are central to the research but not yet described in published literature, software must be made available to editors and reviewers. We strongly encourage code deposition in a community repository (e.g. GitHub). See the Nature Research guidelines for submitting code & software for further information.

Data

Policy information about availability of data

All manuscripts must include a data availability statement. This statement should provide the following information, where applicable:

- Accession codes, unique identifiers, or web links for publicly available datasets
- A list of figures that have associated raw data
- A description of any restrictions on data availability

RNA-seq and DNA-seq datasets have been deposited at GEO (accession number GSE###). Essential plasmids have been deposited at Addgene (plasmid IDs 195237-195242). Unprocessed blots have been included with this article as Source Data. Microscope image files have been deposited at Zenodo (doi ###). The GRCh38 reference genome is publicly available (GENCODE Release 39).

Field-specific reporting

Please select the one below that is the best fit for your research. If you are not sure, read the appropriate sections before making your selection.

☒ Life sciences ☐ Behavioural & social sciences ☐ Ecological, evolutionary & environmental sciences

For a reference copy of the document with all sections, see nature.com/documents/nr-reporting-summary-flat.pdf

Life sciences study design

All studies must disclose on these points even when the disclosure is negative.

Sample size	No sample size calculation was performed for our study. All experiments were performed with three biological replicates, except for RNA-seq and DNA-seq experiments, which were performed once due to time and cost constraints. 100 cells were counted for each microscopy experiment. Sample sizes were chosen based on the standard in the field and prior knowledge of experimental variation.
Data exclusions	No data were excluded.
Replication	All experiments were performed with three biological replicates, except for RNA-seq and DNA-seq experiments, which were performed once due to time and cost constraints. All reported data was reproducible. Means and standard deviations are provided in each figure.
Randomization	Randomization was unnecessary for our study because it is not a subjective trial and the results presented here were purely based on objective and quantitative measurements under controlled conditions. No animal or human subjects were used in this study. Randomization is not typically used for these types of experiments.
Blinding	Blinding was unnecessary for our study because it is not a subjective trial and the results presented here were purely based on objective and quantitative measurements under controlled conditions. No animal or human subjects were used in this study. Blinding is not typically used for these types of experiments.

Reporting for specific materials, systems and methods

We require information from authors about some types of materials, experimental systems and methods used in many studies. Here, indicate whether each material, system or method listed is relevant to your study. If you are not sure if a list item applies to your research, read the appropriate section before selecting a response.

Materials & experimental systems

n/a	Involved in the study
☐	☒ Antibodies
☐	☒ Eukaryotic cell lines
☒	☐ Palaeontology and archaeology
☒	☐ Animals and other organisms
☒	☐ Human research participants
☒	☐ Clinical data
☒	☐ Dual use research of concern

Methods

n/a	Involved in the study
☒	☐ ChIP-seq
☐	☒ Flow cytometry
☒	☐ MRI-based neuroimaging

Antibodies

Antibodies used	Primary antibodies: mouse anti-FLAG (Sigma, F1804, Lot# SLCC6485), rabbit anti-GAPDH (Cell Signaling Technology, 14C10, Lot# 14). Secondary antibodies: IRDye 680RD goat anti-mouse (LI-COR, 926-68070, Lot# C90910-21), IRDye 800CW goat anti-rabbit (LI-COR, 926-32211, Lot# C90723-19), Alexa Fluor 555 goat anti-mouse (Invitrogen, A21424, Lot# 2123594).
Validation	The anti-FLAG and anti-GAPDH primary antibodies have been extensively used in the field and validated by the manufacturer. Please see citations and data on each of the product pages demonstrating antibody validity for the purposes of Western blot and immunofluorescence.

Eukaryotic cell lines

Policy information about cell lines

Cell line source(s)	HEK293T, HEK293T-GFP, and HEK293T-GFP/RFP cells were obtained from the UC Berkeley Cell Culture Facility.
Authentication	All cell lines were authenticated by and purchased commercially from the UC Berkeley Cell Culture Facility.
Mycoplasma contamination	All cell lines were confirmed to be mycoplasma-free (abm, PCR mycoplasma detection kit).

Commonly misidentified lines (See ICLAC register)	No commonly misidentified cell lines were used in this study.

Flow Cytometry

Plots

Confirm that:

☒ The axis labels state the marker and fluorochrome used (e.g. CD4-FITC).

☒ The axis scales are clearly visible. Include numbers along axes only for bottom left plot of group (a 'group' is an analysis of identical markers).

☒ All plots are contour plots with outliers or pseudocolor plots.

☒ A numerical value for number of cells or percentage (with statistics) is provided.

Methodology

Sample preparation	HEK293T cells were trypsinized, quenched in medium, pelleted, resuspended in PBS, and filtered through a 40-micron cell strainer prior to flow cytometry or FACS.
Instrument	Attune NxT acoustic focusing cytometer (Thermo Fisher Scientific); Sony Cell Sorter SH800Z
Software	Attune Cytometric Software v5.1.1; Sony Cell Sorter Software v2.1.5; FlowJo v10.7.1.
Cell population abundance	mCherry-positive (transfected) cells were sorted with an efficiency of >95% prior to downstream analyses.
Gating strategy	1) FSC-A/SSC-A was used to remove debris; 2) FSC-A/FSC-H was used to define single cells; 3) FSC-A/GFP-A or RFP-A was used to determine fluorescence. Gating for RFP-positive (transfected) cells was based on RFP-negative (untransfected) cells. GFP/RFP knockdown was based on cells treated with non-targeting crRNA controls. We have included example gating strategies in Supplementary Fig. 1.

☒ Tick this box to confirm that a figure exemplifying the gating strategy is provided in the Supplementary Information.